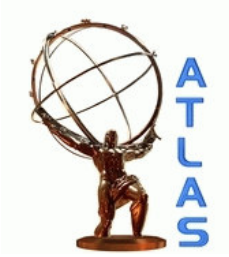

ATLAS NOTE

ATL-PHYS-PUB-2009-000

March 22, 2009

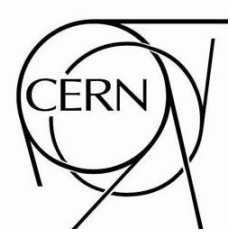

In-Situ Determination of the Performance of the Muon Spectrometer

The ATLAS Collaboration[1)]

This note is part of CERN-OPEN-2008-020. This version of the note should not be cited: all citations should be to CERN-OPEN-2008-020.

ATL-PHYS-PUB-2009-010
24 April 2009

Abstract

The ATLAS muon spectrometer consists of three layers of precision drift-tube chambers in a toroidal magnetic with a field integral between 2.5 and 6 Tm. Muon tracks are reconstructed with 97% efficiency and a momentum resolution between 3% and 4% for 10 GeV$< p_T <$500 GeV and better than 10% for transverse momenta up to 1 TeV. In this note, the performance of a perfectly calibrated and aligned muon spectrometer will be reviewed and the impact of deteriorations of the magnetic field, the calibration and misalignment of the muon chambers on the performance will be discussed. The main part of the note describes how the performance of the muon spectrometer can be determined using dimuon decays of Z bosons and J/ψ mesons.

[1)]This note prepared by C. Amelung, M. Antonelli, F. Bauer, M. Bellomo, N. Benekos, I. Boyko, A. Bruni, L. Chevalier, S. Diglio, A. Eppig, C. Gatti, S. Giovanella, P.-F. Giraud, M. Gostkin, O. Kortner, J.-F. Laporte, D. Levin, G. Maccarone, S. Miscetti, T. Müller, K. Nikolaev, D. Orestano, F. Petrucci, D. Rebuzzi, J. Schmaler, M. Schott, L. Spogli, E. Thompson, V. Tsulaia and S. Willocq.

1 Introduction

Muons with a transverse momentum[2)] p_T greater than 3 GeV are detected in the ATLAS muon spectrometer, which is designed to measure muon momenta with a resolution between 3% and 4% for a range of transverse momenta of 10 GeV$< p_T <$500 GeV and better than 10% for p_T's up to 1 TeV. The muon spectrometer consists of a system of superconducting air-core toroid coils producing a magnetic field with a field integral between 2.5 and 6 Tm [1]. Three layers of chambers are used to precisely measure muon momenta from the deflection of the muon tracks in the magnetic field (see Figure 1). Three layers of trigger resistive-plate chambers (RPC) in the barrel and three layers of fast thin-gap chambers (TGC) in the end caps of the muon spectrometer are used for the muon trigger. The trigger chambers measure the muon tracks in two orthogonal projections with a spatial resolution of about 1 cm. The precision measurement of the muon trajectory is performed by three layers of monitored drift-tube (MDT) chambers in almost the entire muon spectrometer and by cathode-strip chambers (CSC) in the innermost layer of the end caps at $|\eta| > 2.2$. The precision muon chambers provide track points with 35 μm resolution in the bending plane of the magnetic field. The goal of a momentum resolution better than 10% up to 1 TeV scale requires the knowledge of the chamber positions with an accuracy better than 30 μm in addition to the high spatial resolution of the chambers. This is achieved by a system of optical alignment monitoring sensors [1].

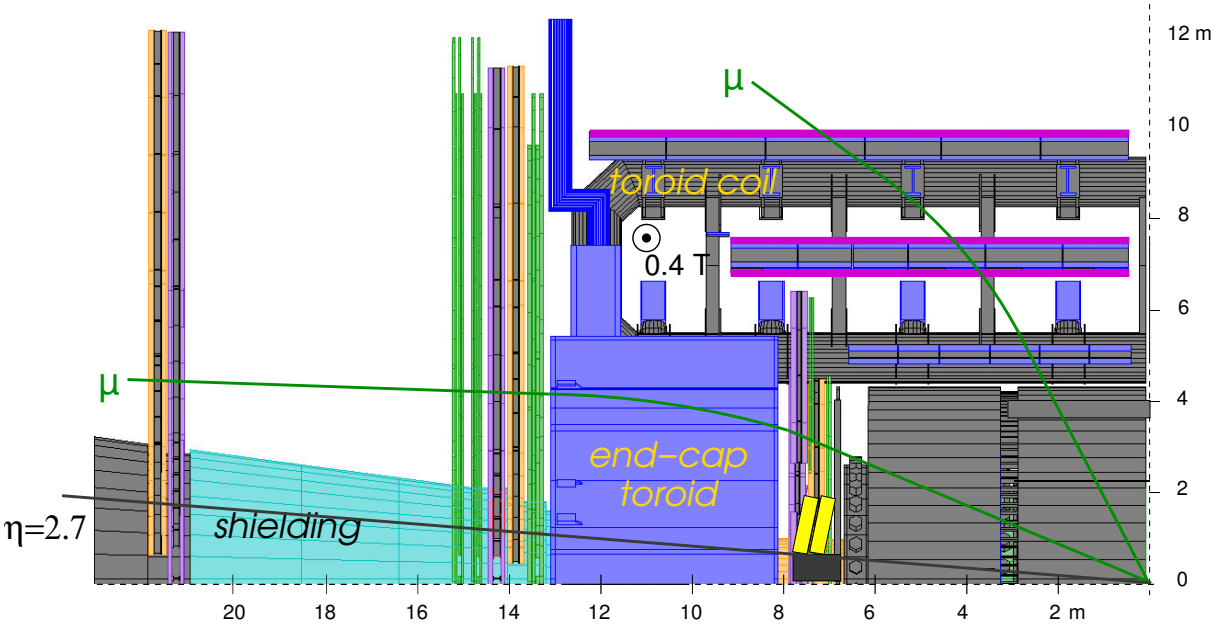

Figure 1: Sketch of a quadrant of the ATLAS muon spectrometer.

In the first part of this note, we review the performance of a perfectly calibrated and aligned muon spectrometer and discuss the dependence of the performance on the knowledge of the following quantities: the magnetic field, the calibration of the chambers, the alignment of the chambers, and the accuracy of the determination of the energy loss of the muons in the calorimeters. In the second and main part, we describe how the performance of the muon spectrometer can be determined by means of dimuon decays of Z bosons and J/ψ mesons.

[2)] The transverse momentum is defined as the components of momentum in the transverse plane.

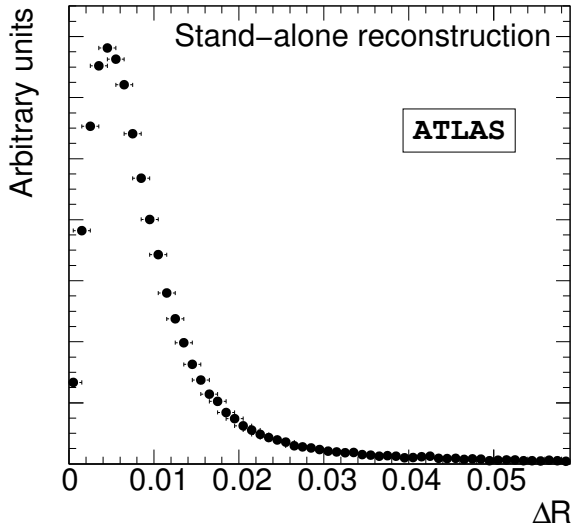

Figure 2: Distribution of distance ΔR of reconstructed from generated muons in a 50 GeV single muon Monte Carlo sample.

2 Performance of a perfect and deteriorated spectrometer

2.1 Muon reconstruction

The muon spectrometer measures the momenta of charged particles at the entrance of the muon spectrometer. The energies lost by the muons on the passage through the calorimeters have to be added to the energy measured at the entrance of the muon spectrometer in order to obtain the muon momentum at the primary vertex. This reconstruction strategy is called *stand-alone* muon reconstruction. In order to correct for the energy loss, the expected average energy loss is used as a first estimation; in a second step the energy deposition measured in the calorimeters is used to account for the large energy losses of highly energetic muons due to bremsstrahlung and direct e^+e^- pair production. One speaks of *combined* muon reconstruction when the momentum measurement of the inner detector is combined with the stand-alone reconstruction. In this note, muon momenta will always be given at the pp interaction point.

The muon reconstruction is described in detail in [2, 3]. The focus of this note is the measurement of the performance of the stand-alone reconstruction from real data.

2.2 Definitions

The performance of the muon spectrometer is characterized in terms of *efficiency* and *momentum resolution*. In the analysis of simulated data, let η_{rec} and η_{truth} denote the pseudorapidities and ϕ_{rec} and ϕ_{truth} denote the azimuthal angles of the reconstructed and generated muons. The distance $\Delta R = \sqrt{(\eta_{rec}-\eta_{truth})^2+(\phi_{rec}-\phi_{truth})^2}$ of a reconstructed and generated muon is shown for a Monte Carlo sample with muons of $p_T = 50$ GeV at the pp interaction point in Figure 2. More than 99.7% of all reconstructed muons have a distance $\Delta R < 0.05$. We therefore define the muon reconstruction *efficiency* as the fraction of generated muons which can be matched to a reconstructed muon within a cone of $\Delta R < 0.05$.

The momentum resolution is measured by comparing the deviation of the reconstructed inverse transverse momentum from the generated inverse transverse momentum:

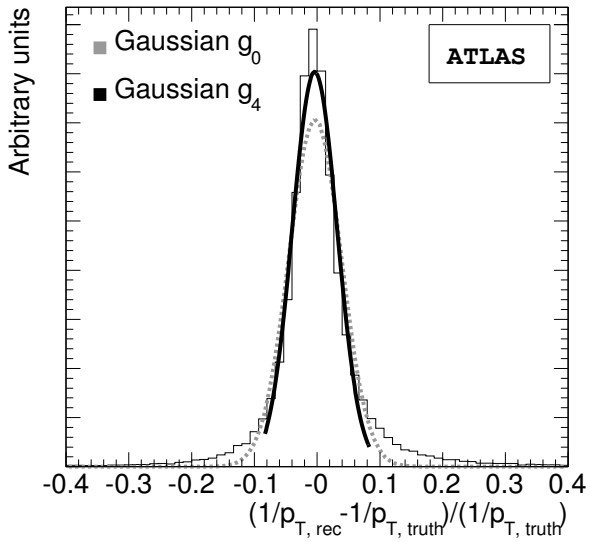

Figure 3: Illustration of the iterative fit of normal distributions to the fractional deviation of the reconstructed inverse momentum from the generated inverse momentum. g_0 is the fitted Gaussian of iteration step 0. g_4 is the fitted Gaussian of final iteration step 4.

$$\rho = \frac{\frac{1}{p_{T,truth}} - \frac{1}{p_{T,rec}}}{\frac{1}{p_{T,truth}}} \tag{1}$$

ρ would be normally distributed for a muon spectrometer uniform in η and ϕ. The momentum resolution is not independent of η and ϕ due to the nonuniformity of the magnetic field and the nonuniformity of the material distribution in η and ϕ. This leads to non-Gaussian tails in the ρ distribution when integrated over η and ϕ, as illustrated in Figure 3. In order to minimize the effect of tails, the momentum resolution is determined in the following way throughout this note: In the first step, a Gaussian g_0 is fitted to the distribution. In the next step i a Gaussian g_i is fitted to the data between the $x_{m,i-1} \pm 2\sigma_{i-1}$, where σ_{i-1} is the fitted width of g_{i-1} and $x_{m,i-1}$ its fitted mean. The iterative procedure is terminated when the fit relative change of the fit parameters from one to the next iteration is less than 0.1%. The standard deviation of the final fit curve is taken as a measure for the *momentum resolution*. The mean of final fit is referred to as the *momentum scale*, which is a measure for systematic shifts of measured muon momenta with respect to the correct values.

2.3 Performance of a perfect muon spectrometer

We briefly review the performance of a perfectly calibrated and aligned muon spectrometer. We refer to [1] and [2] for a more detailed discussion of the performance.

Figure 4(a) shows the reconstruction efficiency for muons with p_T=50 GeV as a function of η and ϕ. The efficiency is close to 100% in most of the η-ϕ plane. It drops significantly in the acceptance gaps of the muon spectrometer. The inefficiency near $|\eta| = 0$ is caused by the gap for services of the calorimeters and the inner tracking detector. The inefficiency near $|\eta| = 1.2$ will disappear after the installation of additional muon chambers in the transition region between the barrel and the end caps which will not be present in the initial phase of the LHC operation. The inefficiencies at $\phi \approx 1.2$ and $\phi \approx 2.2$ for $|\eta| < 1.2$ are related to acceptance gaps in the feet region of the muon spectrometer.

The stand-alone reconstruction efficiency is presented as function of p_T in Figure 4(b). It rises from 0 to its plateau value of 95% between $p_T = 3$ GeV and 10 GeV.

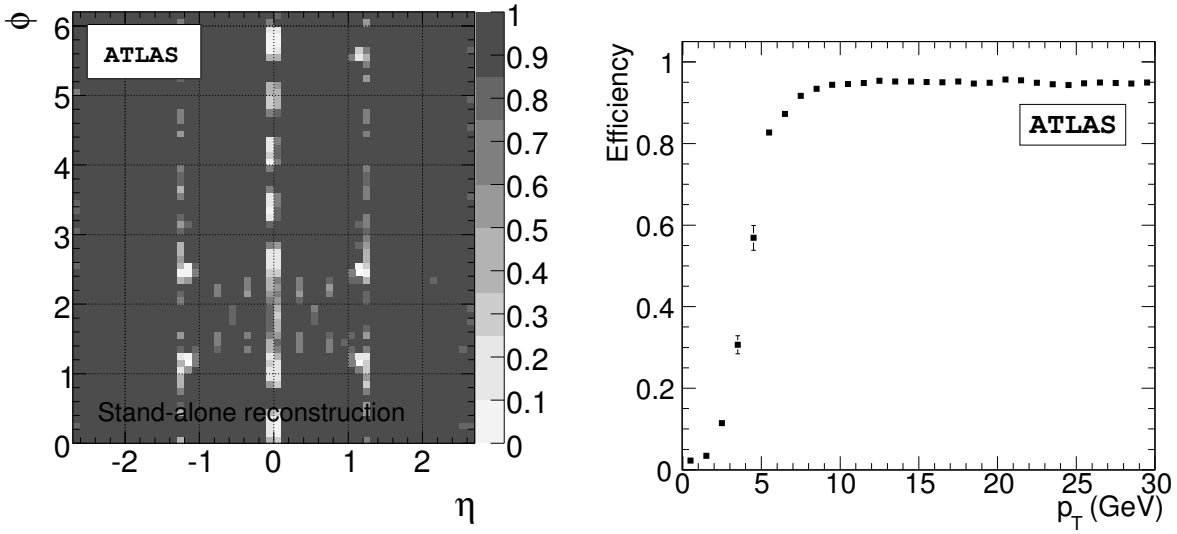

(a) Reconstruction efficiency vs. η and ϕ for muons of p_T=50 GeV.

(b) Reconstruction efficiency vs. p_T integrated over η up to $|\eta| < 2.7$ and ϕ.

Figure 4: Efficiencies of the reconstruction of tracks in the muon spectrometer.

The p_T-resolution is independent of ϕ apart from the feet region where it is degraded due to the material introduced by the support structure of the detector. The resolution also depends on pseudorapidity. It is almost constant in the barrel part of the spectrometer ($|\eta| < 1.05$). It is up to three times worse in the transition region between the barrel and the end caps for $1.05 < |\eta| < 1.7$ mainly due to the small integral of the magnetic field in this region. The momentum resolution becomes uniform again for $|\eta| > 1.7$.

The stand-alone momentum resolution varies with p_T (see Figure 5). The momentum resolution in the barrel is dominated by fluctuations of the energy loss in the calorimeters for $p_T < 10$ GeV where it is about 5% at $p_T = 6$ GeV. It is best, 2.6% (4%) in the barrel (end cap), for $p_T \approx 50$ GeV where it is dominated by multiple scattering in the muon spectrometer. The momentum resolution at high momenta is limited by the spatial resolution and the alignment of the precision chambers and approaches 10% at $p_T = 1$ TeV.

2.4 Deterioration of the performance

The performance of the stand-alone muon reconstruction is affected by the limited knowledge of the magnetic field in the muon spectrometer, the limited knowledge of the material distribution along the muon trajectory required for the calculation of the energy loss, the calibration of the position measurements by the monitored drift-tube chambers, and the alignment of the muon chambers.

The magnetic field will be known with a relative accuracy better than 5×10^{-3} based on the measurements of 1840 magnetic field sensors which are mounted on the muon chambers. As a consequence the relative impact on the momentum resolution is less than 3% [1].

Studies for the technical design report of the muon spectrometer [4], which have been confirmed by

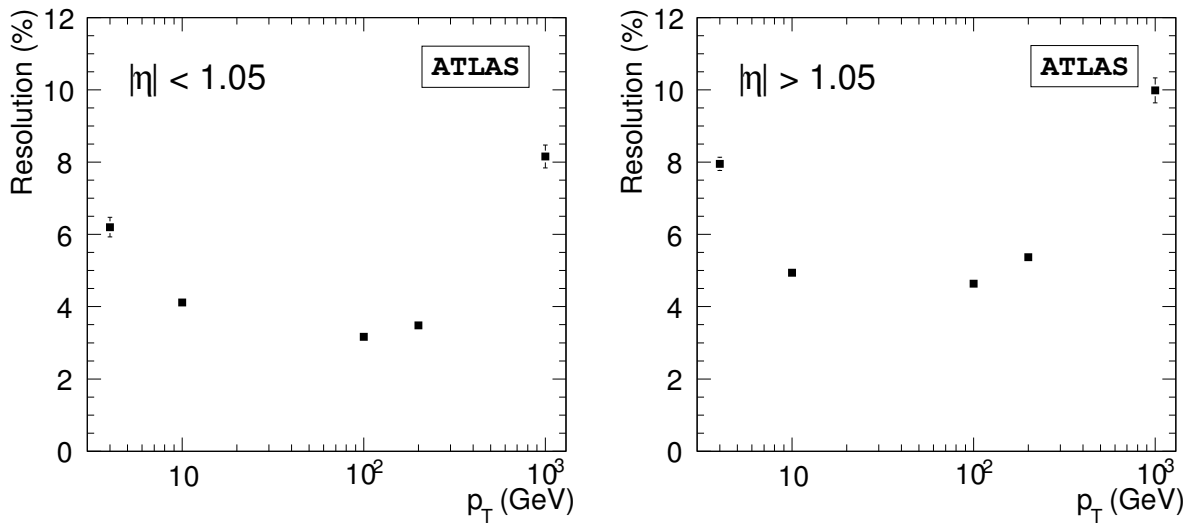

(a) (b)

Figure 5: Stand-alone momentum resolution integrated over η and ϕ as a function of p_T for the barrel (5(a)) and the end-cap region (5(b)).

studies in the context of this note, show that the space-drift-time relationship $r(t)$ of the MDT chambers must be determined with 20 μm accuracy in order to give a negligible contribution to the momentum resolution up to $p_T = 1$ TeV. A strategy to calibrate $r(t)$ with muon tracks with the required accuracy has been worked out and is described in detail in [5].

The muon chambers are installed with a positioning accuracy of 1 mm in the muon spectrometer with respect to global fiducials in the ATLAS cavern. The studies for the technical design report, however, showed that the muon chambers must be aligned with an accuracy better than 30 μm in the bending plane. A bias of 30 μm on the sagitta of a 1 TeV muon corresponds to a systematic shift of the measured momentum of 60 GeV. The alignment of the muon spectrometer is based on a system of optical alignment sensors monitoring relative movements of the chambers on the level of a few micrometers. Muon tracks are used for the absolute calibration of the optical sensor with 30 μm accuracy. The optical system does not cover the whole muon spectrometer. The positions of the end caps with respect to the barrel must be measured with muon tracks traversing the overlap between the barrel and the end-cap part of the spectrometer. There are also chambers in the transition region between the barrel and end caps whose positions are not monitored by the optical system. These chambers will be aligned with the rest of the muon spectrometer by muon tracks. The alignment of the muon spectrometer is discussed in [6].

The expectation of the muon energy loss in the calorimeters can be checked by comparing the muon momentum as measured by the inner detector and the muon momentum at the entrance of the muon spectrometer, for instance. We shall not discuss the measurement of the muon energy loss in this article and refer the reader to [7].

The initial misalignment will be the dominant source of performance degradation. We shall show in the next section that $Z \rightarrow \mu^+\mu^-$ will lead to a clearly visible resonance peak in the dimuon mass distribution even in the case of the initial misalignment. It will therefore be possible to measure the muon performance of a misaligned muon spectrometer with $Z \rightarrow \mu^+\mu^-$ events.

Impact of misalignment on the performance

In order to study the impact of the initial misalignment of the muon spectrometer on the performance, the simulated data were reconstructed with a different geometry from the one used in the simulation. In the reconstruction geometry, the chambers were randomly shifted from the nominal positions with Gaussian distribution centred at 0 and a standard deviation of 1 mm and rotated randomly with Gaussian distribution centred at 0 and a standard deviation of 1 mrad. Deformations of the chambers which are monitored by an optical system mounted on the chambers were not considered in our studies.

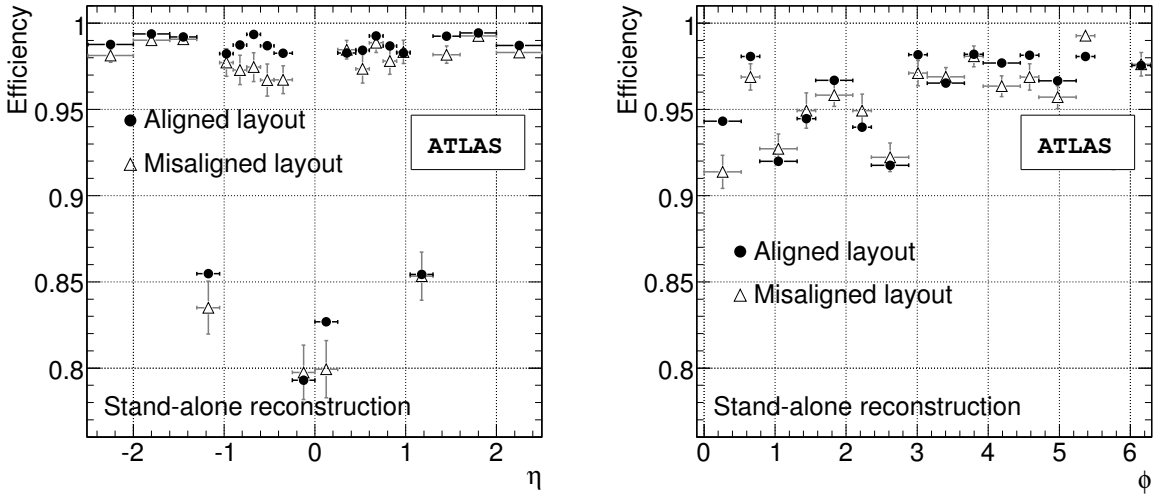

(a) Efficiency vs. η integrated over ϕ for p_T=50 GeV.

(b) Efficiency vs. ϕ integrated over η for p_T=50 GeV.

Figure 6: Comparison of reconstruction efficiency for an aligned muon spectrometer and a misaligned muon spectrometer with a average positioning uncertainty of 1 mm for a simulated single muon sample.

Figure 6 illustrates the comparison of the stand-alone track reconstruction efficiency for 50 GeV muons in the aligned and the misaligned case. Only a small decrease in the reconstruction efficiency can be observed for muons with a momentum of 50 GeV, a momentum typical for muons originating from W or Z bosons. The relatively small decrease in the reconstruction efficiency is mainly due to the fact that the used definition of efficiency is based on a simple η and ϕ matching and does not take into account the measured transverse momentum of the muons. The reconstruction efficiency could be increased in the misaligned case by applying softer cuts in the pattern recognition stage of the track reconstruction.

Figure 7(a) and 7(b) show the impact of a misaligned muon spectrometer on the fractional transverse momentum resolution; the resolution is highly degraded. The overall observed fractional muon spectrometer resolution σ_{tot} can be expressed as the quadratic sum of the intrinsic fractional p_T-resolution at the ideal geometry (σ_{ideal}) and the fractional resolution due to the misaligned geometry ($\sigma_{Alignment}$).

$$\sigma_{tot} = \sqrt{\sigma^2_{Alignment} + \sigma^2_{ideal}}$$

This leads to $\sigma_{Alignment} \approx 0.14$ for muons with $p_T \approx 50$ GeV as expected from the relationship between sagitta and momentum. The effect on the momentum scale is relatively small for the overall muon spectrometer, since random misalignments cancel to a certain extent. In physics signatures, such as the

decay of a Z boson into two muons, the impact on the average momentum scale is even less, since a misaligned geometry has the opposite effect for opposite charged muons to first order.

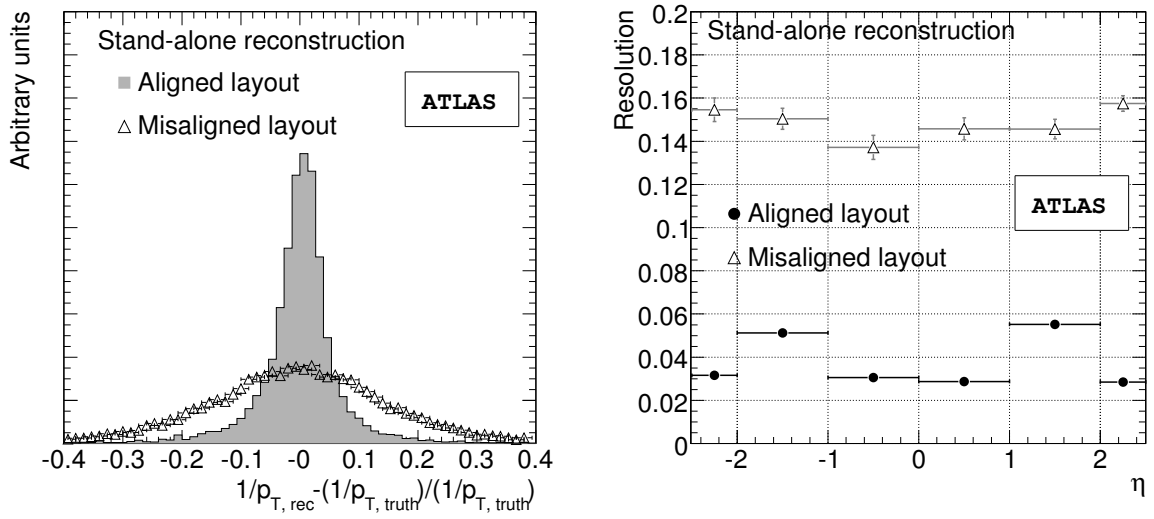

(a) Overall p_T-resolution

(b) p_T-resolution vs. η

Figure 7: Comparison of the fractional p_T-resolution for an aligned muon spectrometer and a misaligned muon spectrometer.

The impact of initial misalignment of the muon spectrometer on the Z resonance is shown in Figure 8. It is expected that the mean of the invariant mass distribution does not change significantly, since the momentum scale of the reconstructed muon p_T is hardly affected by misalignment. On the other hand a large broadening of the distribution due to the degradation of the p_T-resolution of the muons is expected, which is shown in Figure 8. The dependence of the reconstructed width of the Z boson mass distribution on the size of the misalignment is shown in Figure 9. σ_m^{scale} is a scaling factor applied to the initial misalignment of 1 mm and 1 mrad. The observed dependence is the basis for the determination of the muon spectrometer resolution with data, which is discussed in section 4. A more detailed discussion of misalignment impacts on the muon spectrometer performance can be found in [8].

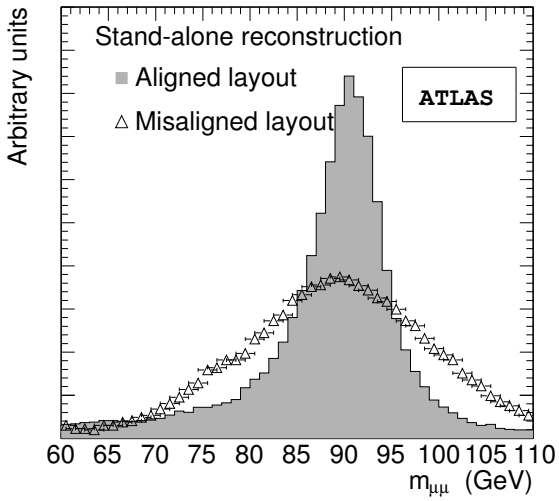

Figure 8: Reconstructed Z boson mass distributions for an aligned and a misaligned ($\sigma_m^{scale} = 1$) muon spectrometer layout.

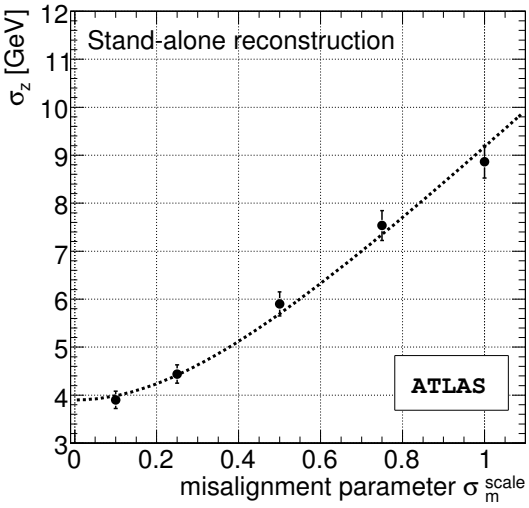

Figure 9: Width of the Z resonance peak including the natural width of the Z vs. misalignment parameter σ_m^{scale}.

3 Measurement of the reconstruction efficiency from pp collision data

The simulation of the ATLAS detector is still under development and is not expected to reproduce the actual performance of the detector in all details at the beginning of the LHC operation. Therefore it is necessary to determine all efficiencies with data in order not to rely on the simulation.

3.1 Reconstruction efficiency from dimuon decays of the Z boson

3.1.1 Tag-and-probe method

The so-called ”tag-and-probe” method can be used to determine the muon spectrometer reconstruction efficiencies from pp collision data. Muons from Z decays will be detected by the inner tracking detector and the muon spectrometer in the common acceptance range of $|\eta| < 2.5$. The measurements of the inner detector and the muon spectrometer are independent, though not necessarily uncorrelated. We require two reconstructed tracks in the inner detector, at least one associated track in the muon spectrometer, and the invariant mass of the two inner-detector tracks to be close to the mass of the Z boson. The last requirement ensures that the reconstructed tracks are the tracks of the decay muons of the Z boson. Moreover, the two inner tracks are required to be isolated to reject possible QCD background. The inner track which could be associated to the track in the muon spectrometer is therefore a muon and is called the *tag muon*. It is also required that the tag muon fired the 20 GeV single-muon trigger in order to ensure that the event is recorded. This selection ensures that a $Z \rightarrow \mu^+\mu^-$ decay has been detected. The second inner track must then be a muon, too, which is called the *probe muon* (see Figure 10). In the analysis of dimuon events from pp collisions, the probe muon plays the role of the generated muon in the determination of the efficiency with simulated data.

The tag-and-probe technique is not restricted to the measurement of the stand-alone reconstruction efficiency. It can, for instance, be used to measure the muon reconstruction efficiency of the inner detector or the trigger efficiency [9].

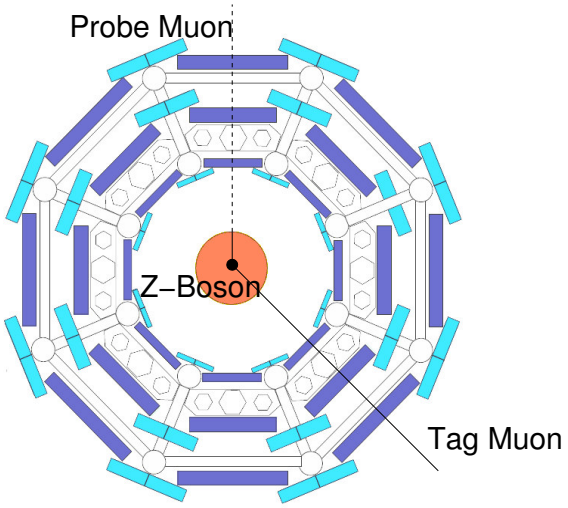

Figure 10: Schematic illustration of the tag and probe method.

Our studies show that the acceptance gaps of the muon trigger which are reflected in uncovered η-ϕ regions of the tag muon do not create uncovered η-ϕ regions of the probe muon. The tag-and-probe method therefore allows us to determine the efficiency over the full η and ϕ coverage of the inner detector.

Some systematic uncertainties of the tag-and-probe method must be considered. Muons from $Z \rightarrow \mu^+\mu^-$ decays usually fly in opposite directions in the plane transverse to the proton beam axis. Hence inefficiencies which are symmetric in $\Delta\phi \approx \pi$ may not be detected with this method.

The topology of $pp \rightarrow Z/\gamma^* \rightarrow \mu^+\mu^-$ events is characterized by two highly energetic and isolated muons in the final state. A significant QCD-background contribution is expected due to the huge cross section of QCD processes. Moreover, the decay of a $W^{\pm}$ boson into one highly energetic muon and a neutrino plus an additional muon from a QCD jet and the process $Z \rightarrow \tau^+\tau^- \rightarrow \mu^+\bar{\nu_\tau}\nu_\mu\mu^-\nu_\tau\bar{\nu_\mu}$ were studied as possible background processes in our analysis.

Because of the high collision energy of the LHC, the production of top quark pairs has a cross section of the order of the signal cross section. Top quarks mostly decay into a W boson and bottom quark. The W boson and the bottom quark can decay into muons or electrons, which also might fake the signal process.

The cross section of QCD processes is far too large to be simulated within a full Monte Carlo simulation of the ATLAS detector. Hence it is assumed that the dominant contribution from highly energetic muons is due to the decay of b-mesons. A more detailed discussion of the selection of $pp \rightarrow Z \rightarrow \mu^+\mu^-$ events and the background processes which must be considered can be found in [9].

3.1.2 Selection of candidate tracks

Figure 11 shows the invariant dimuon mass and the transverse momenta of the selected muon track candidates for the signal and the chosen background processes.

The following cuts have been applied to get a clean track selection. Tracks of opposite charge and a difference in their ϕ coordinates greater than 2.0 rad are selected. The rapidity of the tracks is limited to a rapidity coverage of the inner detector of $|\eta| < 2.5$. Each of the selected muon candidate tracks is required to have $p_T > 20$ GeV. The invariant mass $M_{\mu\mu}$ of the two muon candidate tracks must agree with the Z mass within ± 10 GeV, i.e.$|M_{\mu\mu} - 91.2\,GeV| < 10$ GeV.The following isolation cuts are applied to the selected tracks:

- number of reconstructed tracks in the inner detector within a hollow cone around the candidate muon: $N^{\text{ID Tracks}}_{r_1<r<r_2} < 5$
- sum of the p_T's of reconstructed tracks in the inner detector within a hollow cone around the candidate muon: $\sum_{r_1<r<r_2} p_T^{\text{ID Tracks}} < 8$ GeV
- sum of reconstructed energy in the cells of the calorimeter within a hollow cone around the candidate muon: $\sum_{r_1<r<r_2} E_T < 6$ GeV
- energy of a possible reconstructed jet within a hollow cone around the candidate muon: $E^{\text{Jet Energy}}_{r<r_2} <$ 15 GeV

These isolation variables are defined within a hollow cone in the $\eta-$ and $\phi-$plane of the reconstructed muon track,

$$r_1 < \sqrt{\left(\eta_\mu - \eta_{ic}\right)^2 + \left(\phi_\mu - \phi_{ic}\right)^2} < r_2 \tag{2}$$

where r_1 and r_2 are the inner and the outer radius of the cone. The index μ stands for the reconstructed muon track while the index ic labels the isolation criteria. The smaller radius is set to $r_1 = 0.05$ and is introduced to exclude the candidate muon track from the calculations of the isolation quantities. The specific value of the outer radius r_2 has only a minor effect on the signal and background separation, as long it is large enough to contain a significant amount of data for the definition of isolation variables,

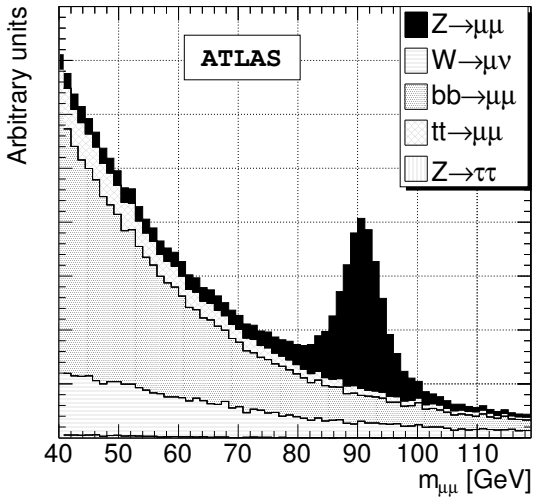

(a) Invariant mass of Z candidates.

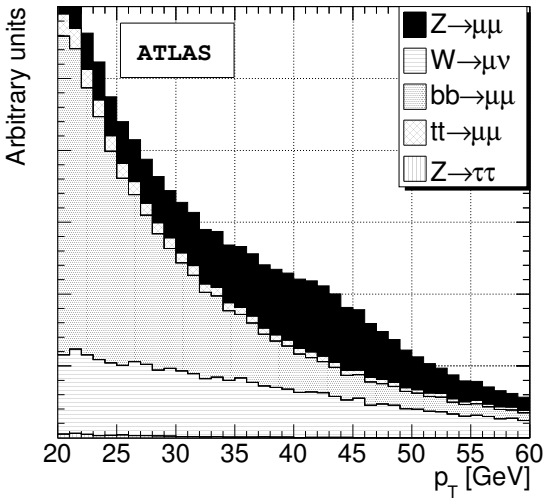

(b) Transverse momentum distribution.

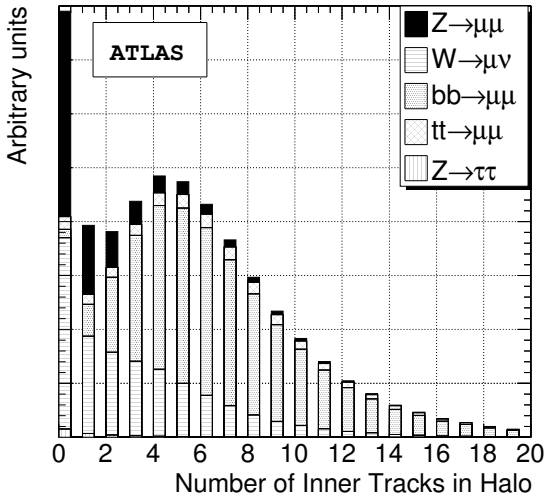

(c) Number of reconstructed tracks within a cone of $\Delta R = 0.5$ around the candidate track.

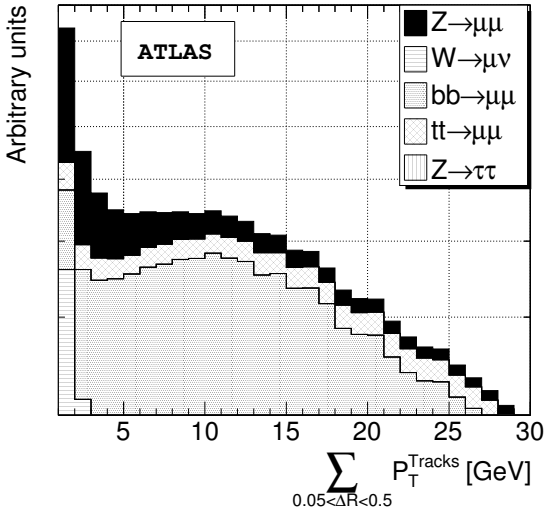

(d) Sum of transverse momenta of all tracks within a cone of $\Delta R = 0.5$ around the candidate track.

Figure 11: Reconstructed quantities for Z candidate events only using inner detector tracks with a transverse momentum above 6 GeV and no further cuts for signal and background processes.

i.e. $r_2 > 0.3$. Our choice of $r_2 = 0.5$ is the same as used in the measurement of the cross section of the process $pp \to Z \to \mu^+\mu^-$ (see [9]). The isolation criteria listed here are optimized for events without pile-up of inelastic pp collisions in a selected event. Pile-up of inelastic pp collisions is expected for the operation of the LHC at a luminosity of 10^{33} cm^{-2} s^{-1} and will lead to more energy in a cone around the muons. It was checked that the efficiency of our event selection is reduced by less than 5% in the presence of pile-up and that the purity of our selected samples is not affected by the presence of pile-up.

The distributions of the first two isolation variables for signal and background processes normalized to their cross sections are presented in Figure 11(c) and 11(d) in absence of pile-up. The selection of isolated high-p_T muons allows for a substantial suppression of the background.

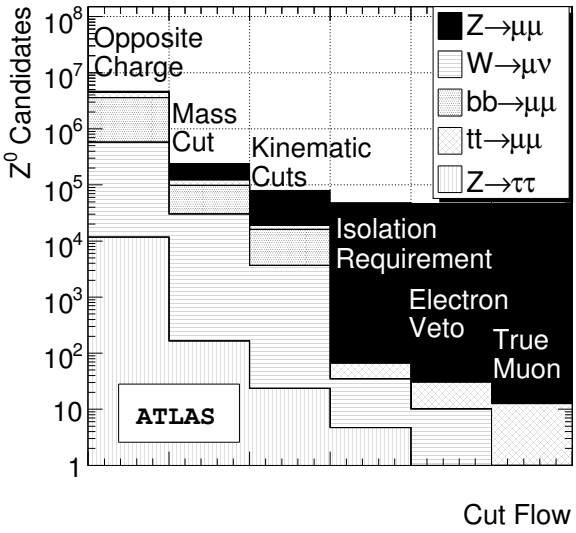

Figure 12: Cut-flow diagram for probe muon tracks: (0) opposite charge requirement, (1) invariant mass requirement, (2) kinematic cuts, (3) isolation requirements, (4) electron veto, (5) found at least one track in the muon spectrometer.

The cut-flow diagram for probe muons is shown in Figure 12. The QCD background can be rejected with isolation cuts. More problematic in this selection is the $W \to \mu\nu$ background, and those $t\bar{t}$-events in which at least one W boson decays into a muon and a neutrino. These processes produce one highly energetic isolated muon track which passes all selection cuts for a tag muon. A further track in the inner detector which passes the other cuts and is not a muon will decrease the measured efficiency. Such a track is most likely caused by an electron, since it is expected that electrons also appear as isolated tracks in the inner detector. Therefore it is required that no reconstructed electromagnetic jet in the electromagnetic calorimeter can be matched to an inner track as an additional selection requirement. This applies especially for probe tracks stemming from a $t\bar{t}$-event. Here, again, one has to distinguish between inner tracks, which result from the decay of the bottom quark or simple QCD-interactions and those, which result from the decay of the W boson. The first case is suppressed by the isolation requirement and can be neglected. The second case can lead to a highly energetic isolated electron, stemming from the decay of the second W boson. These electrons are expected to be vetoed. The cut-flow diagram also shows that the probe muon candidates from the background processes can also be associated to a muon spectrometer track and hence have no negative effect on the efficiency determination.

An overview of the remaining background expected from Monte Carlo is shown in Table 1; there we have assumed at least three events surviving the cuts as a systematic uncertainty in order not to

Table 1: Fractional background contribution in % based on Monte Carlo prediction including estimated systematic and statistical uncertainties.

$b\bar{b} \to \mu\mu$	$W^{\pm} \to \mu^{\pm}\nu$	$Z/\gamma^* \to \tau\tau$	$t\bar{t} \to W^+bW^-b$	Overall
$\approx 0 + 0.03$	$\approx 0 + 0.06$	≈ 0	$\approx 0.02 \pm 0.01$	0.02 ± 0.1

underestimate the background contribution. After all selection cuts, the purity of our sample is high: less than 0.1% of the selected dimuon events are from background processes.

Our results are stable against variations of the track matching distance ΔR from 0.05 to 0.3. The larger track matching cut of ΔR=0.3 takes account for possible misalignment effects in the first phase of LHC. The robustness of our results against the ΔR matching cut indicates that our selected data sample will allow an efficiency determination which is not significantly affected by background processes even with a possible misalignment of the muon spectrometer.

3.1.3 Determination of the stand-alone reconstruction efficiency

The stand-alone reconstruction efficiency depends on p_T, η and ϕ of the muons. Hence, one should determine the efficiency in appropriate bins in these quantities. The lower value of the p_T-binning is given by the selection cut of 20 GeV. The highest value is set to 70 GeV and 10 bins are used to ensure high enough statistics within each bin. For larger statistics also values above 100 GeV can be considered.

A natural binning in η and ϕ is given by the geometry of the muon spectrometer. The muon spectrometer consists of 16 sectors in the ϕ plane, small and large MDT chambers sequentially ordered as illustrated in Figure 13(a). Therefore 16 bins in ϕ are used. The same geometrical argument applies to the η-plane of the detector. Three MDT-chambers which are projective to the interaction point define one tower. Twenty towers are defined in η which are the basis for the chosen binning (Figure 13(b)). In total 320 regions are defined in the $\eta - \phi$ plane.

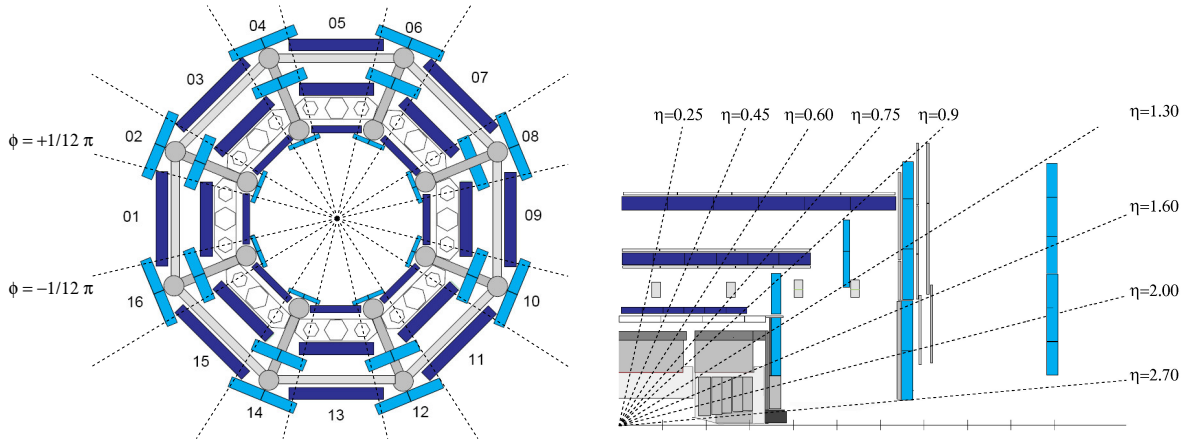

(a) ϕ-binning (b) η-binning

Figure 13: Illustration of the choosen ϕ and η-binning of the muon spectrometer

It is important to note that the dominant effect of losing reconstruction efficiency is the acceptance

Table 2: Overall reconstruction efficiencies for different physics processes. Efficiencies with respect to the Monte Carlo truth information are quoted for the sample of events that pass the single muon trigger.

Sample	$\Delta R = 0.05$	$\Delta R = 0.075$	$\Delta R = 0.15$
$Z \to \mu^+\mu^-$	0.952	0.956	0.958
$W^\pm \to \mu^\pm \nu$	0.953	0.958	0.960
$t\bar{t} \to W^+W^-b\bar{b}$	0.943	0.948	0.950
$b\bar{b} \to \mu^+\mu^-$	0.930	0.944	0.952

gap due to the absence of MDT chambers. Hence it is a pure geometrical effect mainly in the η-direction. Therefore different physics samples with different η- and to a certain extent also different ϕ- and p_T-distributions will lead to different overall reconstruction efficiencies. An overview of the overall reconstruction efficiencies for different physics samples and track matching distances is shown in Table 2. Hence the in-situ determined efficiencies must be applied in an appropriate binning for different physics samples.

The comparison of the efficiencies determined with Monte Carlo truth information and the trag-and-probe method is shown in Figure 14 for η and p_T, assuming an aligned muon spectrometer. A track matching distance of $\Delta R < 0.075$ was chosen. The efficiencies determined in both ways coincide within their statistical uncertainty for an integrated luminosity of 100 pb^{-1}. This proves that possible correlations between tag and probe muons are small and can be neglected to a good extent.

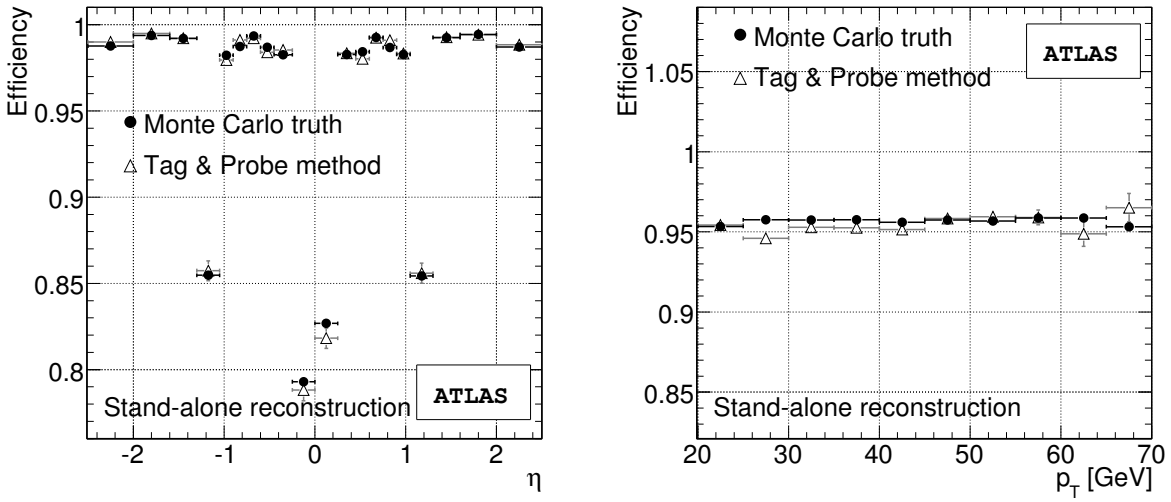

(a) Efficiency integrated over ϕ and p_T in $Z \to \mu^+\mu^-$ events vs. η

(b) Efficiency integrated over ϕ and η in $Z \to \mu^+\mu^-$ events vs. p_T

Figure 14: Comparison of the muon reconstruction efficiency of the muon spectrometer vs. η and p_T determined by the tag and probe method and via the Monte Carlo truth information.

The statistical error on the reconstruction efficiency ε can be calculated (for large N) by

$$\Delta\varepsilon = \sqrt{\frac{\varepsilon(1-\varepsilon)}{N}}, \tag{3}$$

where N is the number of tag muons. Note that both muons can, and will, be chosen as tag muons in most cases, as the muon spectrometer is expected to have a reconstruction efficiency of 95% on average. Figure 15 shows the distribution of the in-situ determined efficiencies for all 320 regions. The overall reconstruction efficiency can be determined to a high statistical precision even for relatively low integrated luminosities. A statistical precision of 1% of the overall muon spectrometer reconstruction efficiency can be reached with less than 1 pb^{-1}. Figure 16 illustrates the statistical uncertainty averaged over all 320 regions versus the integrated luminosity.

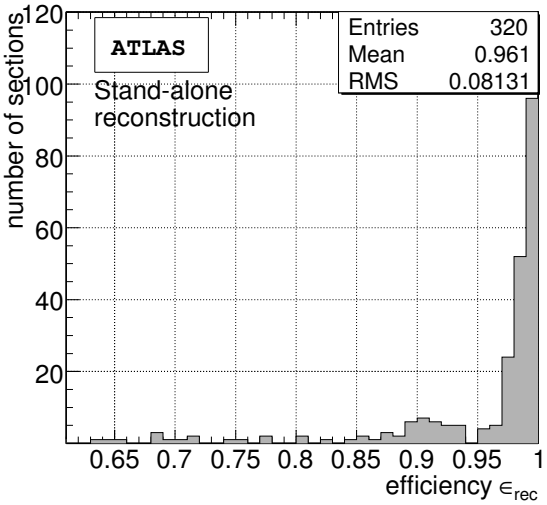

Figure 15: Distribution of muon reconstruction efficiency of the 320 muon spectrometer regions.

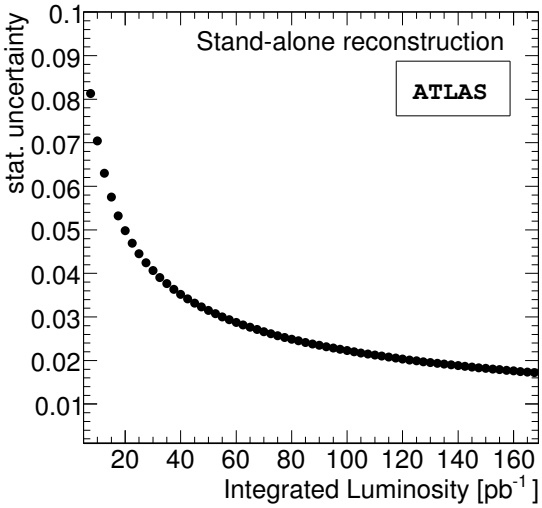

Figure 16: Average statistical error of reconstruction efficiency of the 320 regions vs. integrated luminosity.

A possible correlation between tag and probe muons could be caused by the trigger. The probability of reconstructing a muon is significantly higher if it was triggered, as shown in Figure 17. Hence, it might be suspected that this correlation implies also a correlation in real data, since data events must contain at least one muon which has been triggered. This is not a problem as long as the trigger requirement is only applied on the tag muon.

In Section 3.1.1 it was already mentioned that the tag and probe approach has problems in detecting inefficiencies which have a $\phi \approx \pi$ symmetry. Dividing the data sample in two parts differing in the angle $\Delta\Phi$ could overcome this problem. One part contains reconstructed tag and probe muons with $\Delta\Phi < 2.8$ rad the second sample with $\Delta\Phi > 2.8$ rad. The chosen value of 2.8 rad leads to roughly equally sized samples. Applying the tag and probe method on both sub-samples will lead to different efficiency distributions in case of ϕ-symmetric inefficiencies. Monte Carlo studies showed that for the presently simulated detector layout we expect only small differences (Fig. 18).

Table 3 summarizes statistical and systematic uncertainties of the in-situ determined stand-alone reconstruction efficiency for two different integrated luminosities. The difference in $|\varepsilon_{in-situ} - \varepsilon_{true}|$ is calculated via

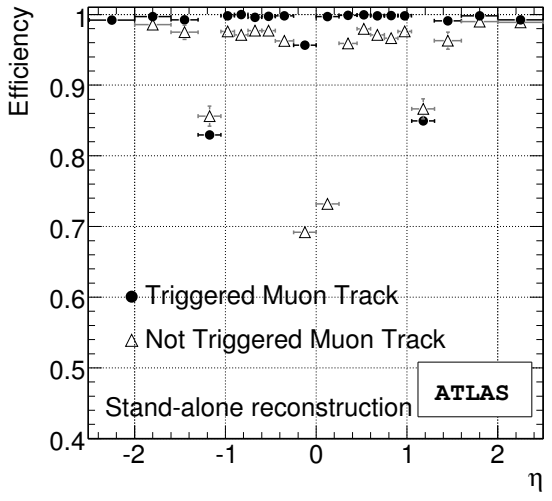

Figure 17: Reconstruction efficiency of the muon spectrometer for muon tracks which have been triggered and muon tracks which have not been triggered.

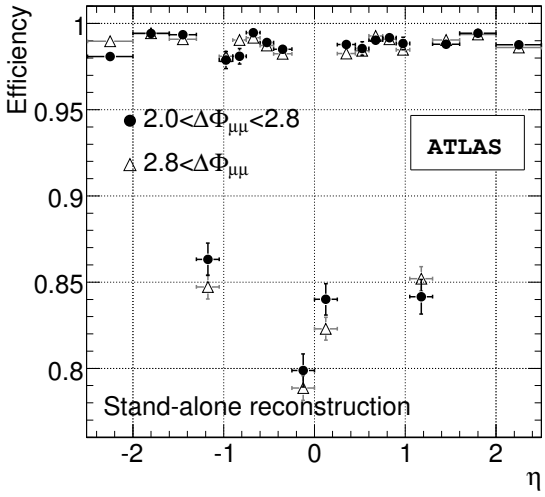

Figure 18: Comparison of muon reconstruction efficiencies determined via tag and probe approach for two sets of muons differing by $\Delta\phi$.

$$|\varepsilon_{in-situ} - \varepsilon_{true}| = \sum_{i=1}^{N} \frac{1}{N} |\varepsilon^{i}_{in-situ} - \varepsilon^{i}_{true}| \tag{4}$$

where the index i runs over all bins in η-direction. This is treated as primary source of systematic uncertainty. One should note that the given systematic error has a strong statistical component from the Monte Carlo statistics which is reflected in the large decrease of the systematic uncertainty in Table 3.

We take the difference between the efficiency obtained for the misaligned layout and the efficiency obtained for the aligned layout as a conservative estimate of the precision which can be achieved with the tag-and-probe method in case of small unresolved misalignments. The difference in both efficiencies for the different $\Delta\phi$-sample is comparable within its statistical uncertainties. The background contribution is only estimated by the Monte Carlo prediction and treated as a systematic uncertainty.

The Gaussian sum of the two systematic uncertainties, namely $|\varepsilon_{in-situ} - \varepsilon_{true}|$ and the background contribution, is defined as the overall systematic uncertainty.

The given uncertainty estimation assumes that nearly all MDT chambers work and $\varepsilon_{true} \approx 96\%$. A lower value of ε_{true} will lead to an increase of the statistical uncertainty via Equation (3) and also to a higher systematic uncertainty. For real data a conservative estimate of the systematic uncertainty would be the difference of the Monte Carlo prediction for the efficiency and the efficiency determined with collision data. Moreover, it should be noted that the given uncertainties apply for muons in a p_T-range between 20 GeV and 60 GeV and within an η-range smaller than 2.5.

3.1.4 Alternative approach

The tag-and-probe analysis presented above uses isolation cuts to reject background events and assumes that a negligable background contribution remains. In this section, we explore the possibility of determining the reconstruction efficiency from collision data without isolation cuts and determine the background

Table 3: Estimated uncertainties of in-situ determined muon spectrometer reconstruction efficiencies for muons in a p_T-range between 20 GeV and 70 GeV and within an η-range smaller than 2.5 from a $Z \to \mu\mu$ decay.

$\int \mathscr{L}$	Statistical Uncertainty	$\lvert\varepsilon_{in-situ} - \varepsilon_{true}\rvert$	Background Contribution	Overall Systematic
100 pb^{-1}	0.08%	0.9%	0.02%	$\approx 1\%$
1 fb^{-1}	0.03%	0.1%	0.02%	$\approx 0.1\%$

contribution directly in data. We apply only cuts on the transverse momenta, e.g. $p_T > 10$ GeV. This leads to a dominant background contribution in the lower invariant dimuon-mass region.

In this approach, a tag muon is defined as a muon spectrometer and inner detector combined muon track, with $p_T > 10$ GeV. A probe muon is defined as any inner detector track, also with $p_T > 10$ GeV. An invariant mass is then calculated from every combinatoric tag and probe pair with opposite charges. The size of this sample is denoted as N in the following (Figure 19(b)). Finally, we select a subsample requiring that the probe muon also be a combined muon track. The size of this sample is denoted as n (Figure 19(a)).

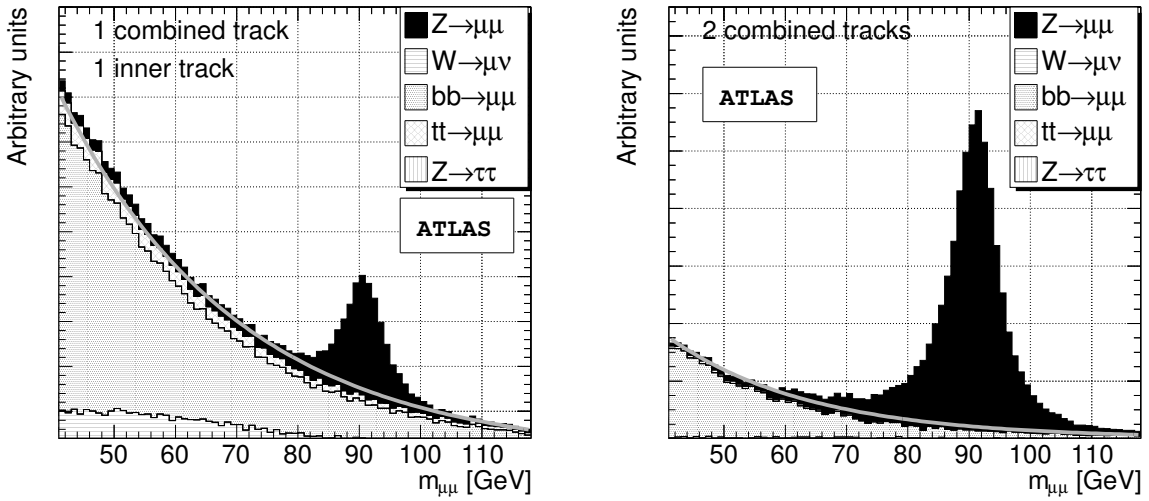

(a) At least one of the muons is matched to a muon spectrometer track.

(b) Both muons are matched to muon spectrometer tracks.

Figure 19: Expected invariant Masses $M_{\mu\mu}$ resulting from two inner tracks where both muons must be matched to a muon spectrometer track (a) or at least one of the muons must be matched to a muon spectrometer tracks (b).

The track-finding effciency of the muon spectrometer, ε, is then defined as n/N. Missing tracks in the muon spectrometer will result in $n < N$ and thus effciency loss. The main difference from the approach presented in Section 3.1 is that no isolation cuts are used for the background rejection but instead the background is directly estimated from data via side band subtraction. In this approach an exponential

function is fitted to the invariant mass region between $\sim$ 40 GeV to $\sim$ 60 GeV, where it is assumed that the background contribution is dominating. The exponential function is then extrapolated to the invariant mass region between $\sim$ 81 GeV to $\sim$ 101 GeV and used for subtraction of the background in this region. The remaining number of events between $\sim$ 81 GeV to $\sim$ 101 GeV define n and N, respectively. In this way, the background contribution is accounted for implicitly in data and no further assumptions on the Monte Carlo predictions are made. The disadvantage of this procedure are the systematic uncertainties of the fitting procedure and the choice of the fitting function. One possible improvement with higher statistics of the background sample would be that the Monte Carlo prediction of the shape of the background distribution could be used to obtain a better fit function than the pure exponential for the side band subtraction.

The systematic uncertainty of this method is again estimated by the residual difference of the in-situ determined efficiency and the true efficiency. For a simulated data sample corresponding to an integrated luminosity of $\int Ldt = 100$ pb^{-1} it is expected to determine the efficiency with this approach up to a precision of

$$\Delta\varepsilon = \pm 0.05(sys.) \tag{5}$$

The relative large systematic uncertainty arises mainly from the limited available statistics of background Monte Carlo samples which has a direct impact on goodness of applied fit. Hence, further improvements are likely to be achieved in future studies.

3.2 Determination of the reconstruction efficiency with J/Ψ events

The reconstruction efficiency for muons with transverse momenta less than 20 GeV is not determined from $Z \to \mu^+\mu^-$ events due to the cuts on the transverse momenta of the muons. Muons from $J/\psi \to \mu^+\mu^-$ decays populate the momentum range below 20 GeV. We explored the possibility of using the tag-and-probe method on $J/\psi \to \mu^+\mu^-$ events for the measurement of the reconstruction efficiency at low transverse momenta. The method works well on signal events. Yet the huge QCD background contaminates the selected dimuon data sets so much that a reliable efficiency measurement becomes very difficult. Studies using muon isolation techniques have started. The muon reconstruction efficiency of low-p_T muons must therefore be extracted from Monte Carlo simulations and not be determined easily from data.

4 Measurement of the momentum resolution and momentum scale

The muon momentum measurement will be affected by the limited knowledge of the magnetic field, the uncertainty in the energy loss of the muons, and the alignment of the muon spectrometer as discussed in Section 2.4.

The analysis of the measurements of the optical alignment sensors and the collision data with the switched-off toroid coils will provide the position of the muon chambers with an accuracy better than 100 μm at the start-up of the LHC [1]. A systematic error of 100 μm on the sagitta corresponds to an additional systematic error in the muon momentum of about 0.1 TeV$^{-1} \cdot p^2$ which amounts to 250 MeV for p=50 GeV.

Muons with energies below 100 GeV lose on average about 3 GeV of their energy on their passage through the calorimeters almost independently of their energy. The material distribution of the ATLAS detector is modelled in the detector simulation with an accuracy better than a few percent [1]. A 5% uncertainty in the amount of the material traversed by the muons would reflect in a 5% uncertainty of the energy loss, that is an uncertainty of the average energy loss of $\pm$150 MeV.

The uncertainty in the bending power of the toroidal field will lead to a momentum uncertainty which is significantly smaller than the energy loss uncertainty and the impact of the misalignment on the momentum measurement. It can therefore be neglected with respect to energy loss uncertainties and the misalignment of the spectrometer.

A bias in the measured muon momentum translates into a bias in the measurement of the dimuon mass in $Z \rightarrow \mu^+\mu^-$ decays. An η, ϕ, and momentum dependent bias will also broaden the dimuon mass peak. The shape of the dimuon invariant mass distribution for $Z \rightarrow \mu^+\mu^-$ decays can therefore be used to measure the accuracy of the momentum measurement with collision data.

As the momentum bias caused by misalignment is of the same magnitude, but of opposite sign for μ^+ and μ^- leptons while the energy loss uncertainty has the same sign and magnitude for μ^+ and μ^- leptons, it is possible to disentangle the effect of misalignment and the effect of energy loss errors on the reconstructed Z mass. The the sensitivities of the dimuon invariant mass spectrum to misalignment and errors in the energy-loss correction were therefore studied separately to get a first insight.

4.1 Determination of the energy-loss uncertainty with $Z \rightarrow \mu^+\mu^-$ events

We begin with the determination of the energy-loss uncertainty with $Z \rightarrow \mu^+\mu^-$ events. We assume that the detector is aligned and that the magnetic field is known with the expected accuracy such that its impact on the momentum scale can be neglected. We allow for an error in the energy-loss and, therefore, correct the reconstructed muon energy in each of the 320 spectrometer towers by a tower-dependent constant $\delta E_{rec,tower}$:

$$E_{rec,tower} \rightarrow E_{rec,tower} + \delta E_{rec,tower}. \tag{6}$$

We determine the 400 constants $\delta E_{rec,tower}$ by minimizing

$$\chi^2 = \sum_{dimuon\ pairs\ k} \frac{[(p_{corr,+,k} + p_{corr,-,k})^2 - M_Z^2]^2}{\sigma_k^2} \tag{7}$$

where $p_{corr,\pm,k}$ denotes the corrected measured $\mu^\pm$ momentum and σ_k the expected dimuon mass resolution. To estimate the sensitivity to the energy-loss correction, we applied this fit to 40,000 simulated $Z \rightarrow \mu^+\mu^-$ events (corresponding to an integrated luminosity of 50 pb^{-1}). The fit gives $\delta E_{rec,tower}$ with a bias of 100 MeV and a stastitical error of the same size. Studies to improve the check of the energy-loss correction with collision data are ongoing.

4.2 Determination of the momentum scale and resolution for a misaligned spectrometer

In a second step, we assume that the energy-loss correction is right and consider the misalignment of the muon spectrometer as the only source of a deterioration of the momentum measurement.

If the Monte Carlo simulation describes the detector correctly, it also predicts the shape of the reconstructed dimuon mass spectrum for $Z \rightarrow \mu^+\mu^-$ events correctly. The misalignment of the muon chambers causes a deviation of the measured from the predicted shape of the invariant dimuon mass spectrum. In order to match the Monte Carlo prediction with the experimental measurement, the reconstructed simulated muon momenta must be smeared and shifted. The following procedure was adopted in our analysis: A random number δp normally distributed around 0 with standard deviation σ_{res} was added to the reconstructed simulated muon momenta $p_{rec,MC}$ and multiplied by a scale factor α:

$$p_{corr} = \alpha(p_{rec,MC} - \delta p). \tag{8}$$

The inclusion of δp corrects for an underestimation of the momentum resolution. The scale factor α takes care of systematic shifts between the reconstructed momenta in the experiment and the simulation.

α and σ_{res} are determined by a fit of the corrected simulated invariant dimuon mass spectrum to the experimentally measured spectrum.

To test this approach, the existing $Z \rightarrow \mu^+\mu^-$ Monte Carlo data set was divided into two subsamples of equal size corresponding to an integrated luminosity of 50 pb^{-1}. The one sample serves as Monte Carlo reference for an aligned muon spectrometer, the other plays the role of the experimental data set. Two scenarios were investigated:

1. The Monte Carlo reference sample and the experimental sample were simulated and reconstructed with the same (aligned) geometry. σ_{res} was fixed to 0 in the analysis of this scenario. Separate scale factors α_B and α_E were applied to muon in the barrel ($|\eta| < 1$) and the end-cap region ($1 \leq |\eta| < 2.7$).

2. The Monte Carlo reference sample was simulated and reconstructed with the same (aligned) geometry. But the experimental sample was reconstructed with a different geometry misaligned as described in Section 2.4. In this scenario, two scale factors α_B and α_E for the barrel and end-cap parts of the muon spectrometer and a global standard deviation σ_{res} were used as fit parameters.

Table 4: Fit results for the scale and resolution parameters for an integrated luminosity of 50 pb^{-1}.

Layout	$1-\alpha_B$	$1-\alpha_E$	σ_{res}
Aligned	$(4\pm14)10^{-4}$	$(1\pm13)10^{-4}$	–
Misaligned	$(6\pm2)10^{-3}$	$(5\pm2)10^{-3}$	(11.6 ± 0.3) %

The results of the tests are summarized in Table 4. In the ideal case in which the reference and the experimental sample are statistically independent, but equivalent otherwise, the fit gives factors α_B and α_E equal to 1 within the statistical errors as expected. In the second scenario, the uncorrected misalignment in the experimental sample leads to a systematic shift of the reconstructed momenta, hence α_B and α_E differ from 1 slightly, but significantly, and a large degradation of the momentum resolution from 3.5% to 12% is observed which is consistent with the degradation presented in Section 6. A large $Z \rightarrow \mu^+\mu^-$ sample would clearly allow for a finer segmentation than the division in barrel and end-cap parts for the scale factors and lead to smaller values of σ_{res}.

The mean value of $1+\frac{p_{corr}-p_{rec,MC}}{p_{rec,MC}}$ is presented in Figure 20 as a function of η for the second scenario. The mean values are spread around 1 with a standard deviation of 0.3%. The maximum deviation from 1 is less than 1%. This results indicates that the Z-mass distribution permits the detection of imperfections in the momentum reconstruction. Studies which use a more refined parametrization of the momentum correction and take into account energy-loss and alignment corrections at the same time are in progess.

We conclude from the studies in this section that it should be possible to control the muon momentum and energy scale on the level of 0.5 GeV for 50 GeV muons with 40,000 $Z \rightarrow \mu^+\mu^-$ events corresponding to an integrated luminosity of 50 pb^{-1}.

5 Conclusions

The performance of the ATLAS muon spectrometer can be predicted by Monte Carlo simulations. The performance of the spectrometer will, however, differ from the prediction due to the initial misalignment of the muon chambers and imperfections in the corrections of the muon energy-loss. It is therefore important to measure the performance with collision data.

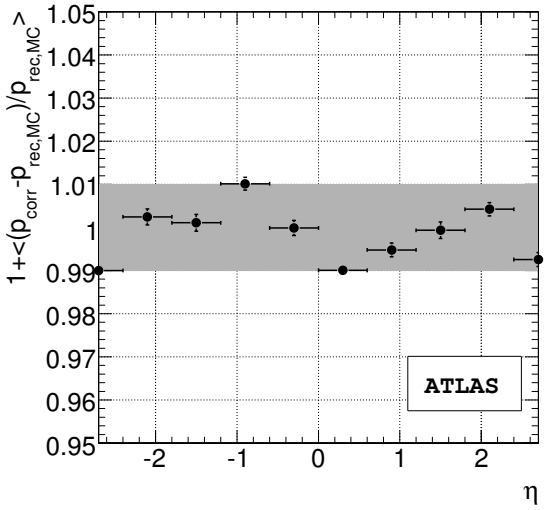

Figure 20: Dependence of $< p_{corr} - p_{rec,MC} > / p_{rec,MC}$ on η integrated over p_T and ϕ for $Z \to \mu^+\mu^-$ events in the second scenario of a misaligned detector.

We showed in the present article that it is possible to measure the muon reconstruction efficiency with $Z \to \mu^+\mu^-$ events with an accuracy better than 1% with an integrated luminosity of 100 pb^{-1}. Selection cuts and the p_T spectrum of the Z decay muons limit the momentum measurement to range of 20 GeV$< p_T <$70 GeV. The efficiency measurement can be extended to higher momenta with increased luminosity when the tails of the p_T spectrum get populated.

We explored the possibility of measuring the efficiency at low transverse momenta with $J/\psi \to \mu^+\mu^-$ events. Our studies show that a reliable efficiency measurement will be difficult due to large irreducible QCD background.

We finally addressed the question of how the momentum and energy scale can be measured with $Z \to \mu^+\mu^-$. According to our feasibility study it will be possible to control the energy-loss correction on the level of 100 MeV and the momentum scale on the level of 1% for an integrated luminosity of about 100 pb^{-1}. More detailed studies are needed to obtain a better estimate of the achievable precision.

References

[1] The ATLAS Collaboration, The ATLAS Experiment at the CERN Large Hadron Collider, JINST 3 (2008) S08003.

[2] The ATLAS Collaboration, Muon Reconstruction and Identification: Studies with Simulated Monte Carlo Samples, this volume.

[3] The ATLAS Collaboration, Mouns in the Calorimeters: Energy Loss Corrections and Muon Tagging, this volume.

[4] The ATLAS Muon Collaboration, ATLAS Muon Spectrometer Technical Design Report, CERN/LHCC 97-22.

[5] P. Bagnaia et al., Calibration model for the MDT chambers of the ATLAS Muon Spectrometer, to be submitted to JINST.

[6] J.C. Barriere et al., The alignment system of the barrel part of the ATLAS muon spectrometer, to be submitted to JINST.

[7] The ATLAS Collaboration, Muons in Calorimeters: Energy Loss Corrections and Muon Tagging, to be submitted to JINST.

[8] N. Benekos et al., Impacts of misalignment on the muon spectrometer performance, ATL-MUON-PUB-2007-006.

[9] The ATLAS Collaboration, Electroweak Boson Cross-Section Measurements, this volume.